Modeling of Bolted Connections for Collapse Analysis of Steel Structures

Joseph A. Main and Fahim Sadek
Engineering Laboratory, National Institute of Standards and Technology, Gaithersburg, MD

INTRODUCTION

In structural collapse scenarios, beam to column connections can be subjected to large rotations as the structure deforms, in addition to large axial forces associated with the development of catenary action. The capability of the connections to sustain large rotations and axial forces can be a critical factor in whether alternate load paths can be developed, bridging over failed members. Because of this, it is important in structural collapse analysis that the interaction of bending moment and axial force, and their combined effects on connection performance, be represented accurately.

The National Institute of Standards and Technology (NIST) is conducting research to develop reliable methodologies for assessing the vulnerability of structures to disproportionate collapse and for quantifying the reserve capacity and robustness of structures at the system level. This research involves the development of three-dimensional models of various types of structural systems, which must be capable of representing the predominant response characteristics and failure modes of each structural system. This paper focuses on the development of models of steel bolted connections for collapse analysis. Both single-plate shear connections and moment connections with bolted webs are considered, with the primary focus being on the behavior of the bolted shear tabs, which exhibit a combination of bolt shear and bearing-induced deformations. Detailed and reduced finite element models of these connections are presented, and results of the computational models are compared with published experimental data to provide validation of the modeling approaches. The reduced models can be analyzed much more rapidly than the detailed models, making them particularly valuable for collapse analysis of complete structural systems.

PROTOTYPE BUILDING DESIGNS

Working with a panel of practicing structural engineers across the U.S., NIST developed the overall configuration and dimensions of prototype buildings to be considered in this research program. For simplicity of design and analysis, a 10-story building with rectangular plan for office occupancy was chosen as the prototype building. Figure 1 shows the plan layout of two prototype steel frame building designs, each having plan dimensions of 30.5 m × 45.7 m. The two different plan layouts shown in Figure 1 were developed to examine the influence of span length on disproportionate collapse resistance. Both buildings were designed for Seismic Design Category C, and the lateral loads are resisted by seismically designed intermediate moment frames (IMFs) located on the exterior of the buildings. All interior frames were designed to support gravity loads only.

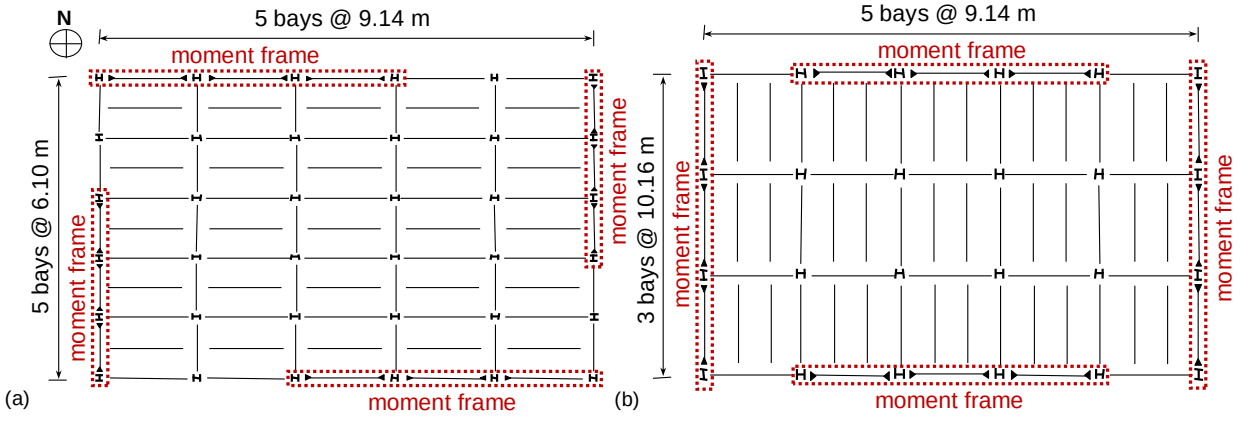

Figure 1. Plan layouts for (a) 5 bay × 5 bay building and (b) 5 bay × 3 bay building.

Approved for public release; distribution is unlimited.

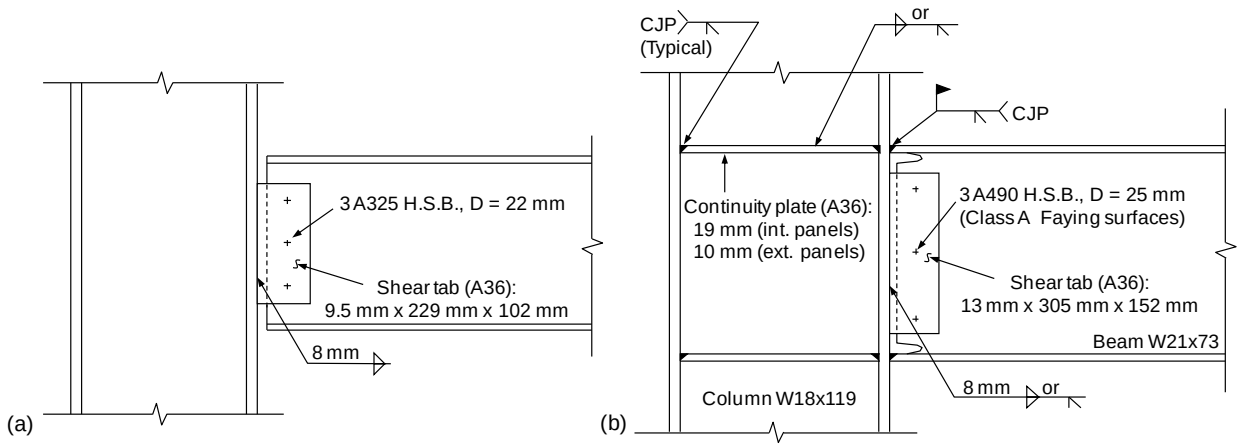

Figure 2. Details of bolted connections: (a) single-plate shear connection; (b) WUF-B moment connection.

The buildings were designed according to the American Society of Civil Engineers 7-02 standard [1] and its referenced material design standards, including the American Institute of Steel Construction (AISC) "Load and Resistance Factor Design Specification for Structural Steel Buildings" [2] and the AISC "Seismic Provisions for Structural Steel Buildings" [3]. Single-plate shear connections with ASTM A325 high-strength bolts (H.S.B.), as shown in Figure 2(a), were used in the gravity frames. The single-plate shear connections in the 5 bay × 5 bay building required three bolts, as shown in Figure 2(a), while those in the 5 bay × 3 bay building required four bolts. Welded unreinforced flange, bolted web (WUF-B) connections with ASTM A490 high-strength bolts, as shown in Figure 2(b), were selected from the prequalified steel connections in FEMA 350 [4] for the intermediate moment frames. The WUF-B connection shown in Figure 2(b) is a second-floor connection in the north-south moment frame of the 5 bay × 5 bay building [Figure 1(a)]. The number and size of the ASTM A490 bolts varied for the WUF-B connections within the moment frames, as did the thickness and height of the shear tab. ASTM A992 structural steel (F_y = 344.8 MPa) was used in all beams and columns. ASTM A36 steel (F_y = 248.2 MPa) was used for the shear tabs and continuity plates at beam-column connections.

MODELING APPROACHES

Two basic modeling approaches can be considered for collapse analysis of structural systems: (1) detailed finite element modeling, which uses highly refined solid and/or shell element meshes to represent nonlinear material behavior and fracture, and (2) reduced finite element modeling, which uses a much smaller number of beam and spring elements to capture the predominant response characteristics and failure modes. Reduced models can be analyzed much more rapidly than detailed models, making them well suited for collapse analysis of complete structural systems. The following sections describe detailed and reduced modeling approaches for the bolted connections shown in Figure 2. Both detailed and reduced models were analyzed using LS-DYNA [5] with explicit time integration.

Detailed Models

The detailed model of the single-plate shear connection, shown in Figure 3(a), consists of finely meshed solid elements representing the beam, shear tab, and bolts. A typical element size of 3 mm was used to represent the beam and shear tab, with three layers of solid elements for the beam web and flanges and four layers of solid elements for the shear tab. A typical solid element size of 1.6 mm was used to represent the bolts. The column flange was modeled using a coarser solid element mesh and is not shown in the figure. Contact was defined between the bolts, shear tab, and beam web to model the transfer of forces through the bolted connection, including friction and bolt bearing.

The detailed model of the WUF-B connection [Figure 3(b)] uses a similar approach to represent the beam, shear tab, and bolts, with a solid element mesh having a comparable level of refinement. Finely meshed solid elements were also used to represent the column, the continuity plates, and the welds connecting the beam flanges to the column. For both the WUF-B and the single-plate shear connection, the shear tabs were modeled as rigidly connected to the column flanges, because hand calculations confirmed that failure of the fillet weld connecting the shear tab to the column flange was not a governing limit state.

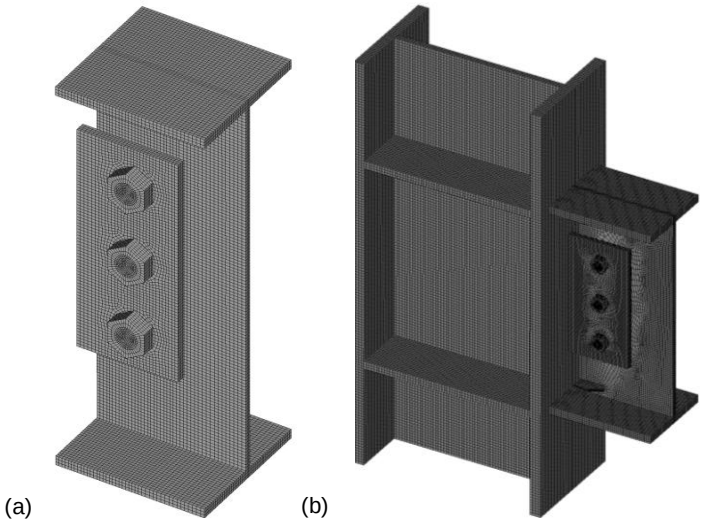

Figure 3. Detailed models of (a) single-plate shear connection (column omitted) and (b) WUF-B connection (b).

A piecewise-linear plasticity model (material 24 in LS-DYNA, [5]) was used to represent the material behavior of the various steel components in the detailed models. In this model, an effective stress versus effective plastic strain curve is specified, along with a plastic strain to failure. Fracture is simulated using element erosion, in which elements are removed from the model when the specified failure strain is reached. The material model parameters for each component were developed based on engineering stress-strain curves obtained from tensile tests. The engineering stress-strain curves were converted to true stress vs. plastic strain curves, and the resulting true stress-strain curves were extrapolated linearly beyond the point of necking onset. The post-necking tangent modulus and the failure strain were adjusted to achieve quantitative agreement between measured and calculated engineering stress-strain curves in the softening region beyond the ultimate stress. Due to mesh-size sensitivity in the modeling of softening behavior, finite element models of tensile coupons were developed using the same mesh size and type (shell or solid element) as those used in the various models of the test specimens for each steel type. This approach ensured that the measured nonlinear material behavior up to failure was accurately captured in the material model.

For the ASTM A325 and A490 high-strength bolts, the material model parameters were based on typical engineering stress-strain curves reported in Kulak et al. [6] and shown in Figure 4(a). Also shown in Figure 4(a) are engineering stress-strain curves computed from detailed solid-element models of tensile coupons with a gage length of 51 mm. The good comparison of the computed and typical stress-strain curves in Figure 4(a) shows that the piecewise linear plasticity model with element erosion accurately represents softening behavior after the onset of necking and captures fracture of the tensile coupons at the appropriate values of engineering strain. Figure 4(b) shows a detailed model of a tensile coupon after fracture with contours of effective plastic strain.

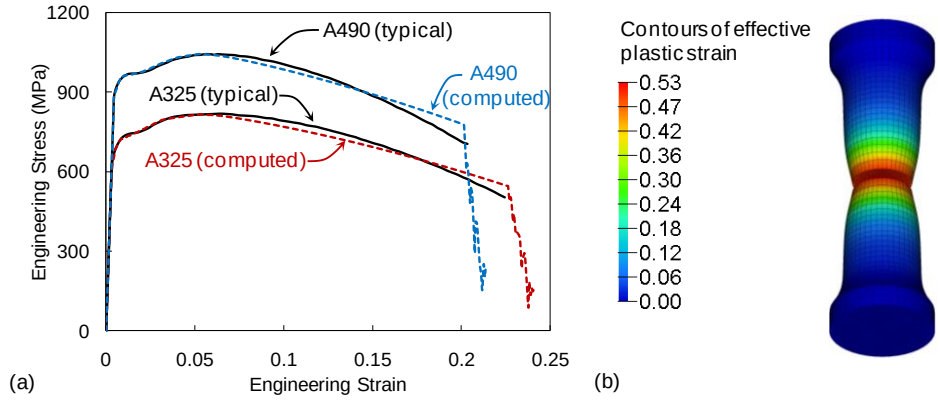

Figure 4. (a) Comparison of computed and typical (from Ref. [6]) engineering stress-strain curves for A325 and A490 high-strength bolt material; (b) detailed model of tensile coupon after fracture.

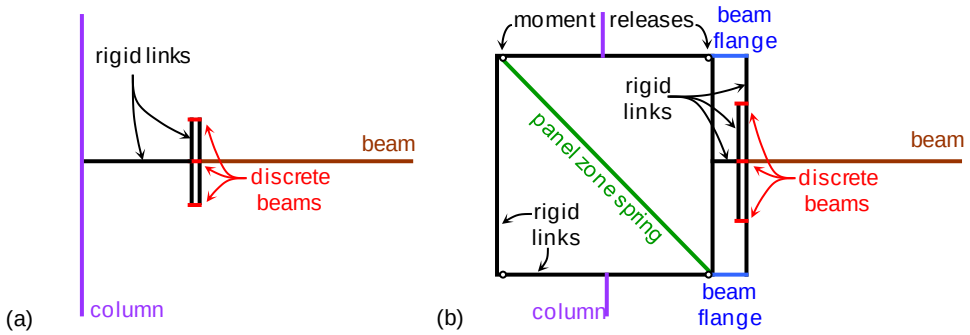

Figure 5. Reduced models of (a) single-plate shear connection and (b) WUF-B connection.

Reduced Models

The reduced model of the single-plate shear connection, shown in Figure 5(a), uses zero-length discrete beam elements [shown with finite length in Figure 5(a) for clarity] to represent the combination of bolt shear and bearing-induced deformation associated with each bolt. Using material model 119 in LS-DYNA [5], two distinct load-deformation curves were defined for each discrete beam element to represent yielding and failure (1) along the beam axis and (2) in the vertical direction. Figure 6(a) shows a simplified piecewise-linear load-deformation curve used to represent yielding and failure of a single-plate shear connection in the axial direction. This simplified piecewise-linear curve is based on the results of a detailed solid-element model of the connection illustrated in Figure 6(b), and the load-deformation curve obtained from this model is shown with the simplified curve in Figure 6(a). The load-deformation behavior of the discrete beam elements in the axial direction captures the interaction of bending moment and axial force for the connection, while the load-deformation behavior in the vertical direction captures vertical shear. To maintain the proper connection geometry, rigid links connect the ends of the discrete beam elements to nodes along the beam and column centerlines. The beam and column are represented using Hughes-Liu beam elements with cross-section integration [5]. A piecewise linear plasticity model was used to represent the steel material of the beam and column, with stress-strain curves based on tensile test data and fracture modeled using element erosion.

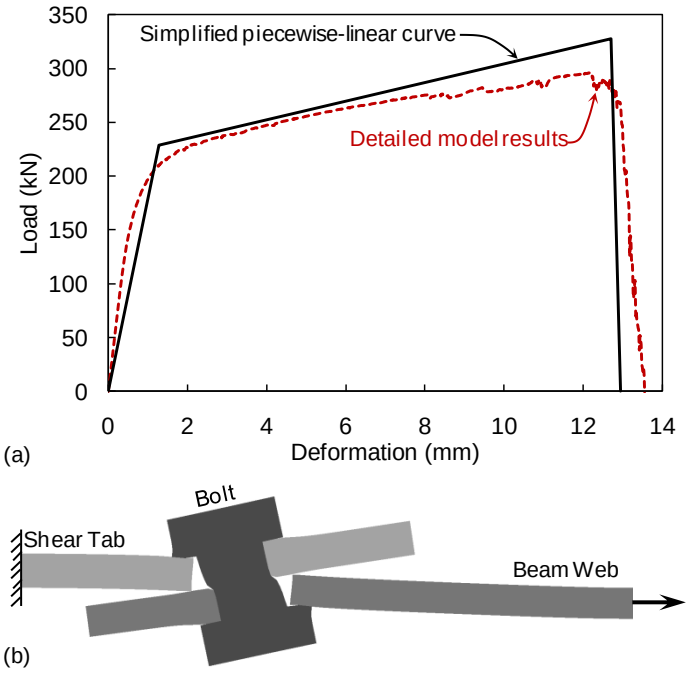

Figure 6. (a) Load-deformation curves for bolted shear connection; (b) section view of detailed finite element model at ultimate load.

The reduced model of the WUF-B connection, shown in Figure 5(b), uses the same approach just described to represent the shear tab bolted to the beam web, with a discrete beam element corresponding to each bolt in the connection. Hughes-Liu beam elements with cross-section integration [5] were used to represent the welded beam flanges, as well as the gross column and beam sections outside of the connection region. Rigid links were used to represent the column flanges and continuity plates in the panel zone, and shear deformations of the panel zone were represented using a diagonal spring with an elastic, perfectly plastic load-displacement curve. The stiffness and yield strength of the panel zone spring were calculated using equations given in [7].

EXPERIMENTAL VALIDATION

To develop confidence in the detailed and reduced modeling approaches, model predictions are compared with available experimental results. First, predictions of the detailed model are compared with experimental data from connections with a single bolt, including double-shear tests, a test of bolt bearing on a single plate, and a single-shear test. Both the detailed and reduced model predictions are then compared with experimental results from a full-scale beam-column assembly incorporating WUF-B connections under a simulated column removal scenario.

Double-Shear Tests

Wallaert and Fisher [8] present results of double-shear tests for high-strength bolts of different materials and sizes, as well as for different plate materials. Detailed models of selected test specimens from Ref. [8] were developed. Because the test configuration was symmetric, only one half of each test specimen was modeled, with appropriate boundary conditions on the plane of symmetry. Figure 7(a) shows a section view of the detailed model of a test specimen at its ultimate load. Figure 7(b) shows the solid element mesh of the bolt after fracture.

Figure 8 shows a comparison of experimental shear stress versus deformation curves with those computed using the detailed model. Generally good agreement is observed for the different combinations of bolt size, bolt material, and plate material, demonstrating that the detailed modeling approach is able to capture the influence of these factors on the strength and ductility of the connections. The ultimate strength obtained from the model is within 6 % of the measured value, while the post-ultimate displacement corresponding to 90 % of the ultimate strength is within 11 %. The initial stiffness computed by the detailed model is consistently lower than that observed experimentally because frictional clamping due to initial bolt tension was not included in the model. However, the initial bolt tension has little effect on the ultimate strength and displacement of the connection, which is of primary interest in this study.

Comparison of Figure 8(a) and Figure 8(b) shows the influence of bolt material, with the A490 bolt exhibiting higher strength than the A325 bolt, with comparable deformations at the ultimate stress. Comparison of Figure 8(b) and Figure 8(d) shows the influence of bolt diameter, with the 25 mm bolt sustaining larger deformations than the 22 mm bolt before failure, with comparable values of the ultimate stress. Comparison of Figure 8(c) and Figure 8(d) shows the influence of plate material, with larger deformations sustained for A440 steel plates than for higher strength quenched and tempered steel plates. The larger deformations for the A440 steel plates were associated with larger bearing-induced deformation of the plates. The detailed model of the plates was able to capture these bearing-induced deformations using a stress-strain curve based on the reported yield and ultimate strengths of 296 MPa and 524 MPa, respectively, for the A440 steel plate. The quenched and tempered steel plates were represented using an elastic material model, to preclude bearing-induced plastic deformations. For all specimens, the ultimate limit state was bolt shear failure, resulting in a rapid drop in resistance after the ultimate stress was reached.

Figure 7. Detailed model of bolt double-shear test: (a) section view at ultimate load; (b) bolt mesh after fracture.

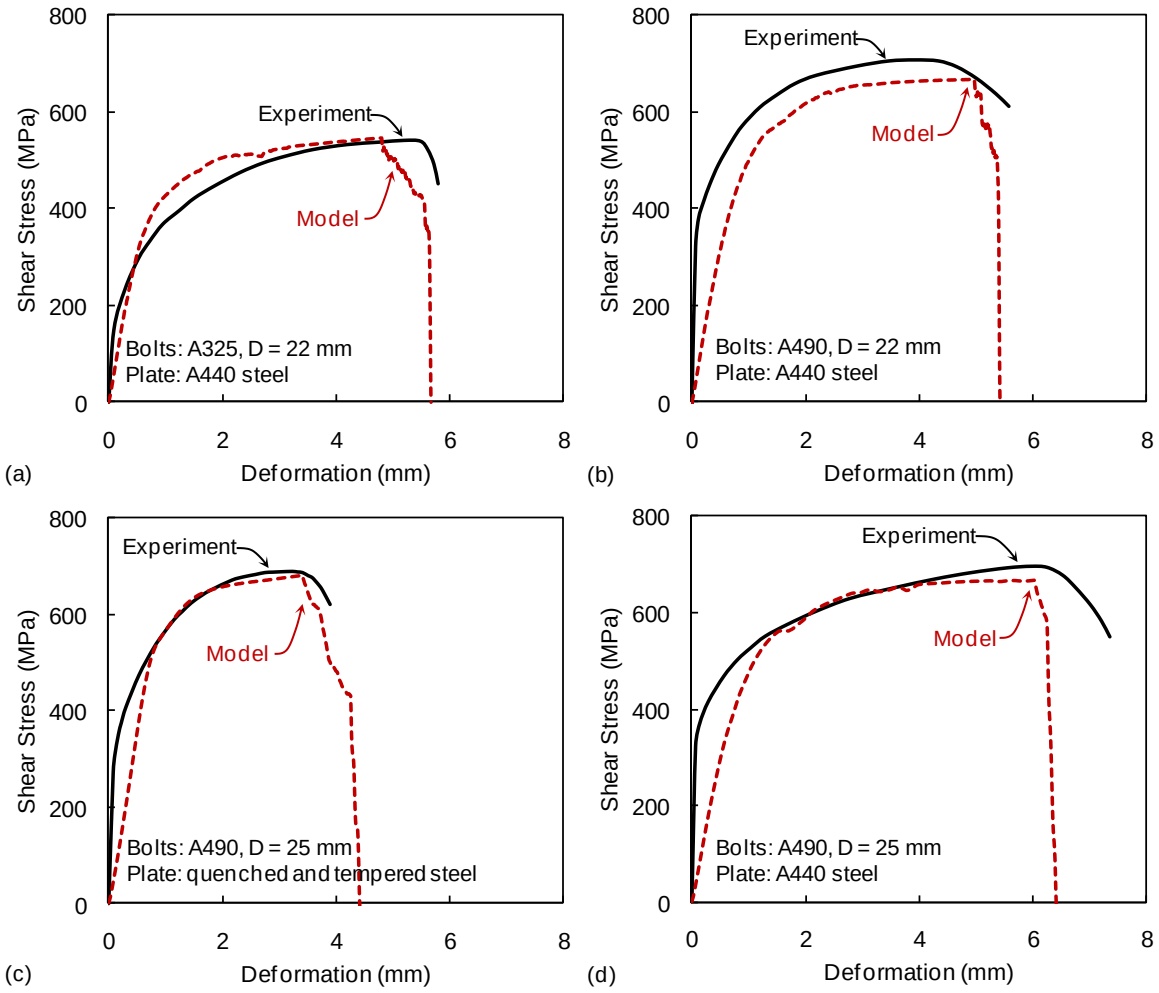

Figure 8. Shear stress versus deformation curves from double-shear specimens: comparison of computed results from detailed models with experimental results from Wallaert and Fisher [8]. (Experimental curves are best-fit to data from several tests; estimated coefficient of variation in measurements: 4 %.)

Bolt Bearing Test

Figure 9(a) shows an experimental load-deformation curve for a bolt bearing a single plate (from Rex and Easterling [9]) compared with results from a detailed model. Figure 9(b) shows the detailed model at the ultimate load of the specimen, in which significant bearing-induced deformations are evident and the associated plastic strains are indicated. The results correspond to a bolt diameter of 25 mm, plate thickness of 6.5 mm, plate width of 127 mm, and a distance of 38 mm from the center of the bolt hole to the edge of the plate. The stress-strain curve for the plate material was based on the reported yield and ultimate strengths of 307 MPa and 452 MPa, respectively. Generally good agreement in the experimental and computed load-deformation curves is observed, and the ultimate load obtained from the model is within 11 % of the measured value. While the experimental curve terminates at a deformation of 12.7 mm (this value of deformation was used to define bearing failure in Ref. [9]), the computational analysis was continued further, showing that the drop in resistance associated with bolt bearing failure and tearout is much more gradual than that associated with bolt shear failure (see Figure 8). The resistance of the connection drops to near zero at a deformation of 36.5 mm, corresponding closely to the edge distance of 38 mm.

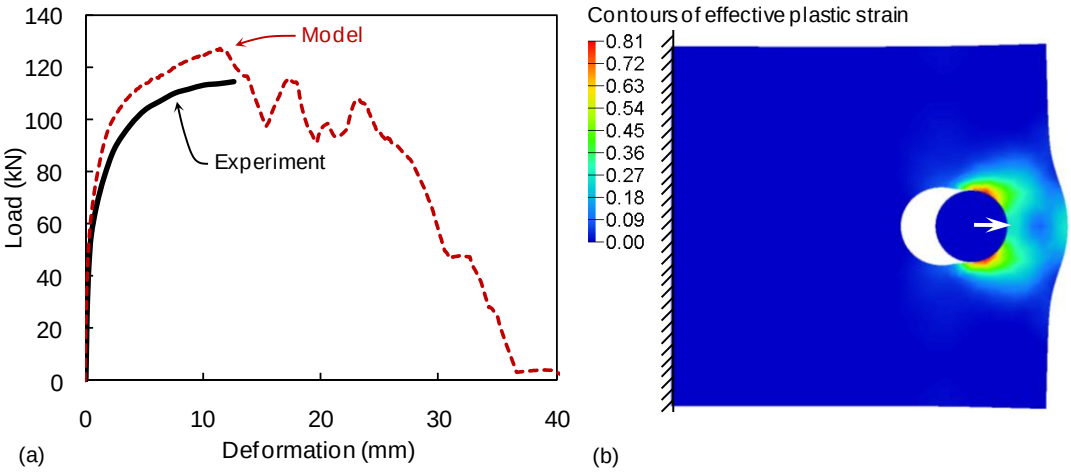

Figure 9. (a) Load-deformation curves for bolt bearing: comparison of detailed model results with experimental data from Rex and Easterling [9]; (b) contours of effective plastic strain from detailed model at ultimate load. (Estimated coefficient of variation in measurements: 0.8 %)

Single-Shear Test

Figure 10(a) shows an experimental load-deformation curve from a single-shear test reported in Richard et al. [10], plotted with computed results from a detailed model. The single-shear test specimen consisted of two 9.5 mm thick A36 steel plates connected by a single 19 mm A325 bolt, with plate widths of 102 mm, and a distance of 38 mm between the center of each bolt hole and the edge of the plate. Figure 10(b) shows a section view of the detailed model at the ultimate load of the specimen. Because the yield and ultimate strengths of the A36 steel plate material were not reported in Ref. [10], minimum specified values of 250 MPa and 400 MPa, respectively, were used in the model. An initial bolt tension consistent with that reported in Ref. [10] was applied in the model by defining a thermal expansion coefficient for the bolt and reducing the bolt temperature to develop the preload. Applying this preload allowed for good agreement in the initial stiffness of the specimen, as shown in Figure 10(a). The computed ultimate load is within 0.5 % of the measured value. While the experimental load-deformation curve terminates at a deformation of 9 mm (a deformation of 7.6 mm was used as the criterion for desired ductility in Ref. [10]), the computational analysis was continued further, showing additional displacement associated with the combined effects of bolt shear and bearing-induced plate deformations [see Figure 10(b)]. The final sudden drop in resistance was associated with bolt shear failure.

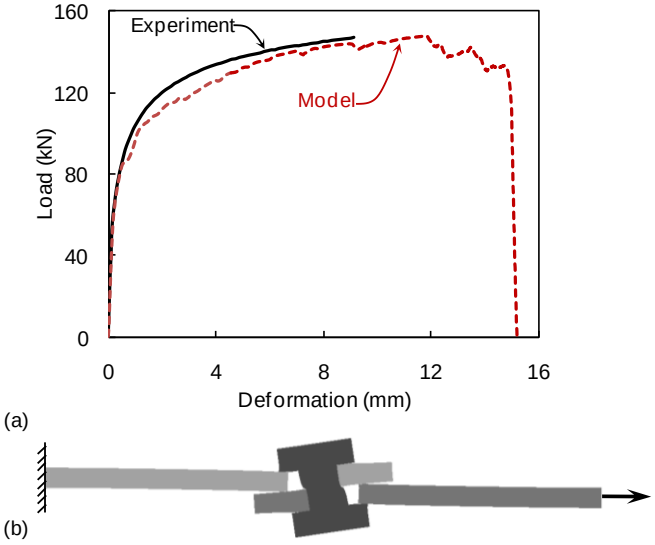

Figure 10. (a) Load-deformation curves for single-shear specimen: comparison of detailed model predictions with experimental results from Richard et al. [10]; (b) section view of detailed model at ultimate load. (Experimental curve is best-fit to data from several tests; estimated coefficient of variation in measurements: 3 %.)

WUF-B Connections under a Column Removal Scenario

Computational results from both the detailed and reduced models are finally compared with experimental data from Sadek et al. [11] for a beam-column assembly with WUF-B connections under a simulated column removal scenario. The full-scale test specimen, shown schematically in Figure 11 and further described in Ref. [11], consisted of two beam spans connected to three columns by WUF-B connections. The top of each end column was restrained by two diagonal braces to simulate the bracing effect provided by the upper floors in a multi-story building. The unsupported center column was forced downward by a hydraulic ram under displacement control until a failure mechanism of the assembly was reached. Both detailed and reduced models of the assembly were developed, using the detailed and reduced modeling approaches described above and shown in Figure 3(b) and Figure 5(b), respectively. In the detailed model, coarser shell elements were used to represent the beams and columns away from the connection regions, where yielding was not expected, as described in Ref. [11]. In both the detailed and reduced models, the column bases were represented as perfectly fixed.

Figure 12 shows (a) the applied vertical load and (b) the beam axial force plotted against the vertical displacement of the center column, comparing the results of the detailed and reduced models with the experimental measurements. While the reduced model uses far fewer elements than the detailed model, the results show that it is capable of capturing the primary response characteristics of the test specimen.

Consistent with the experimental results, the results of the detailed and reduced models shown in Figure 12(a) indicate that the assembly remained in the elastic range up to a vertical displacement of the center column of about 50 mm. The analyses indicate that in the early stages, the behavior of the assembly was dominated by flexure, as indicated by the relatively small axial compression in the beams shown in Figure 12(b). With increased vertical displacement of the center column, axial tension developed in the beams and the behavior was dominated by catenary action. The axial tensile force in the beams increased with increased downward displacement of the center column, as Figure 12(b) indicates, until a WUF-B connection at the center column could no longer carry the combined axial and flexural stresses, resulting in the failure of the assembly.

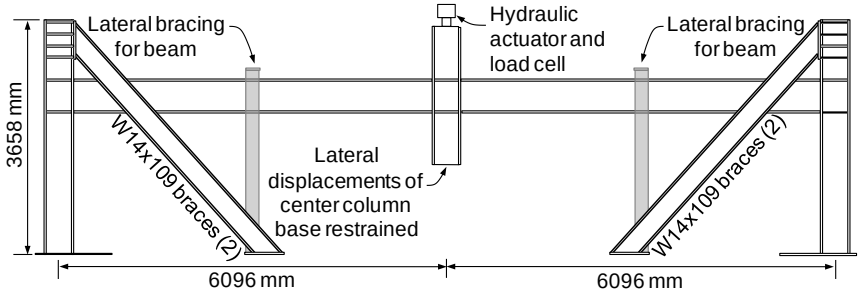

Figure 11. Test configuration for steel beam-column assembly with WUF-B connections.

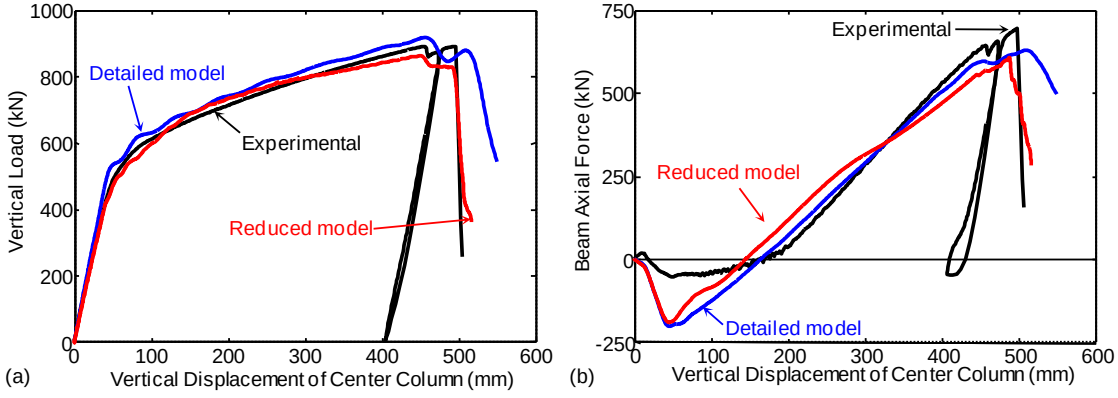

Figure 12. Comparison of experimental and computational results for beam-column assembly with WUF-B connections: (a) applied vertical load and (b) beam axial force versus vertical displacement of center column. (Estimated coefficient of variation in measurements: 1 %.)

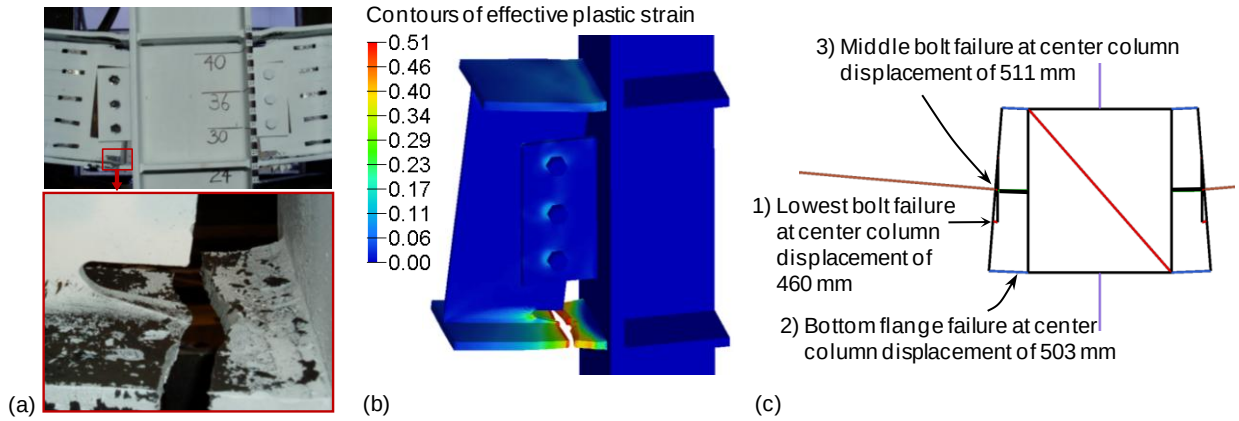

Figure 13. Failure mode of WUF-B connection at center column: (a) photographs of test specimen; (b) detailed model; (c) reduced model.

The failure mode of the WUF-B connection to the center column is shown in Figure 13(a) and was characterized by the following sequence: (1) local buckling of the top flanges of the beams near the center column, (2) successive shear failure of the lowest and middle bolts connecting the beam web to a shear tab at the center column, and (3) fracture of the bottom flange near the weld access hole. The computed failure mode from the detailed model, shown in Figure 13(b), was very similar to that observed in the experiment. The lowermost bolt connecting the beam web to the shear tab at the center column failed in shear at a vertical displacement of the center column of about 445 mm, which was immediately followed by failure of the middle bolt. The bottom flange of the beam near the weld access hole began to fracture at a center column vertical displacement of approximately 483 mm. The fracture initiated at the root of the access hole (center of flange) and propagated outward until the bottom flange completely fractured. The computed failure sequence from the reduced model is indicated in Figure 13(c). The lowermost bolt connecting the beam web to the shear tab failed first, and was followed by the nearly simultaneous failures of the middle bolt and the bottom flange of the beam. This failure sequence is generally consistent with what was observed in both the experiment and the detailed model.

SUMMARY AND CONCLUSIONS

Motivated by the need to model the behavior of steel beam-to-column connections under the large rotations and axial forces that can be developed in collapse scenarios, this paper presented detailed and reduced modeling approaches for bolted connections. Single-plate shear connections were considered, as well as WUF-B moment connections, which incorporate a shear tab bolted to the beam web. The detailed modeling approach used highly refined solid elements to represent nonlinear material behavior and fracture, while the reduced modeling approach used a much smaller number of beam and spring elements. In the reduced modeling approach, discrete beam elements were used to represent each bolt in the connection, with load-deformation curves that incorporate the combined effects of bolt shear and bearing-induced deformations. These load-deformation curves were based on the results of detailed models, so experimental validation of the detailed modeling approach is of fundamental importance to establish confidence in both detailed and reduced models.

To provide experimental validation, computational results from the detailed models were compared with experimental data in the literature for connections with a single bolt, including double-shear tests, a bolt tearout test, and a single-shear test. Good overall agreement was observed between the experimental and computational results. The important role of bearing-induced deformations in achieving a ductile response was evident, and connections with bolt tearout as the governing limit state exhibited a much more gradual reduction in resistance after the ultimate load than connections governed by bolt shear failure. Computational results from both the detailed and reduced models were also compared with experimental results for a beam-column assembly incorporating WUF-B connections under a simulated column removal scenario. Both the detailed and reduced models were able to accurately represent the primary response characteristics and failure modes of the assembly, including the development of catenary action and the ultimate failure of a WUF-B connection to the center column due to successive fractures of bolts and the lower flange of the beam. The reduced models can be analyzed much more rapidly than the detailed models and will be useful in assessing the vulnerability of complete structural systems to disproportionate collapse.

DISCLAIMER

Certain commercial entities, equipment, products, or materials are identified in this document in order to describe a procedure or concept adequately. Such identification is not intended to imply recommendation, endorsement, or implication that the entities, products, materials, or equipment are necessarily the best available for the purpose.

REFERENCES

1. American Society of Civil Engineers (ASCE). (2002). "Minimum design loads for buildings and other structures." *SEI/ASCE 7-02*, Reston, VA.
2. American Institute of Steel Construction (AISC). (1999). "Load and resistance factor design specifications for structural steel buildings." Chicago, IL.
3. American Institute of Steel Construction (AISC). (2002). "Seismic provisions for structural steel buildings." *ANSI/AISC 341-02*, Chicago, IL.
4. Federal Emergency Management Agency (FEMA). (2000a). "Recommended seismic design criteria for new steel moment-frame buildings." *FEMA 350*, SAC Joint Venture and FEMA, Washington, D.C.
5. Hallquist, J. (2007). "LS-DYNA Keyword User's Manual." Livermore Software Technology Corporation, Livermore, CA.
6. Kulak, G. L., Fisher, J. W., and Struik, J. H. A., (1986). *Guide to Design Criteria for Bolts and Riveted Joints*, 2nd Ed., John Wiley & Sons, New York.
7. Khandelwal, K., El-Tawil, S., Kunnath, S.K., Lew, H.S. (2008). "Macromodel-based simulation of progressive collapse: steel frame structures." *Journal of Structural Engineering*, 134(7), 1070-1078.
8. Wallaert, J.J., and Fisher, J.W. (1965). "Shear strength of high-strength bolts." *Journal of the Structural Division, ASCE*, Vol. 91, ST3, 99-125.
9. Rex, C.O., and Easterling, S.W. (2003). "Behavior and modeling of a bolt bearing on a single plate." *Journal of Structural Engineering*, 129(6), 792-800.
10. Richard, R.M., Gillett, P.E., Kriegh, J.D., and Lewis, B.A. (1980). "The analysis and design of single plate framing connections." *Engineering Journal, AISC*, 2nd Quarter, 38-52.
11. Sadek, F., Main, J.A., Lew, H.S., Robert, S.D., Chiarito, V.P., El-Tawil, S. (2010). "An Experimental and Computational Study of Steel Moment Connections under a Column Removal Scenario." *NIST Technical Note 1669*, National Institute of Standards and Technology, Gaithersburg, MD.